PCCP

PAPER

View Article Online
View Journal | View Issue



Cite this: *Phys. Chem. Chem. Phys.*, 2015, **17**, 19360

# Mechanism for formation of atmospheric Cl atom precursors in the reaction of dinitrogen oxides with HCl/$Cl^-$ on aqueous films†

Audrey Dell Hammerich,*[a] Barbara J. Finlayson-Pitts[b] and R. Benny Gerber[bcd]

Received 8th May 2015,
Accepted 22nd June 2015

DOI: 10.1039/c5cp02664d

www.rsc.org/pccp

Nitryl chloride ($ClNO_2$) and nitrosyl chloride (ClNO) are potential sources of highly reactive atmospheric chlorine atoms, hence of much interest, but their formation pathways are unknown. This work predicts production of these nitrogen oxychlorides from *ab initio* molecular dynamics (AIMD) simulations of $N_2O_5$ or an $NO_2$ dimer on the surface of a thin film of water which is struck by gaseous HCl. Both of these heterogeneous reactions proceed at the liquid/vapor interface by an $S_N2$ mechanism where the nucleophile is chloride ion formed from the ionization of HCl on the aqueous surface. The film of water enhances the otherwise very slow gas phase reaction to occur by (1) stabilizing and localizing the adsorbed $N_2O_5$ or $NO_2$ dimer so it is physically accessible for reaction, (2) ionizing the impinging HCl, and (3) activating the adsorbed oxide for nucleophilic attack by chloride. Though both nitrogen oxychloride products are produced by $S_N2$ reactions, the $N_2O_5$ mechanism is unusual in that the electrophilic N atom to be attacked oscillates between the two normally equivalent $NO_2$ groups. Chloride ion is found to react with $N_2O_5$ less efficiently than with $N_2O_4$. The simulations provide an explanation for this. These substitution/elimination mechanisms are new for $NO_{x/y}$ chemistry on thin water films and cannot be derived from small cluster models.

## Introduction

Chlorine atoms gained notoriety with their catalytic effect on the depletion of the earth's stratospheric ozone layer and are implicated in a host of tropospheric reactions.[1–7] They are a highly reactive species which can be readily produced during the photolysis of an otherwise stable Cl containing compound. Given the abundance of HCl (and chloride ion) along with various oxides of nitrogen in the atmosphere, their ability to react and form a photolyzable Cl containing species could have significant ramifications for atmospheric chemistry. The formation of nitryl chloride ($ClNO_2$), a potential Cl radical precursor, from $N_2O_5$ and HCl had been suggested[8] and it was found as a product in the reaction of $N_2O_5$ with HCl/ice surfaces.[9] Extensive laboratory studies have shown that nitryl chloride can be formed through the heterogeneous reaction of $N_2O_5$ with sea salt aerosols, both dry NaCl surfaces[10–13] and wet surfaces.[14–17] Almost two decades after the first study was reported, the relevance of these reactions was finally underscored when advances in analytical methodology enabled the direct observation and quantification of $ClNO_2$ in a marine environment.[18] More recent laboratory studies indicate that $ClNO_2$ can also form through the reaction of $N_2O_5$ with wet or dry HCl in a process where water assumes a catalytic role.[19] Field studies confirm nitryl chloride in ambient air in inland as well as marine locations on a number of continents.[20–27] The incorporation of $ClNO_2$ into large-scale atmospheric models suggests that nitryl chloride may have a significant impact upon Cl radical formation and atmospheric oxidative chemistry.[28,29] Additional laboratory studies have shown that another potential Cl atom precursor, nitrosyl chloride, can also form from heterogeneous reactions of wet and dry NaCl, this time when the sea salt aerosol comes in contact with $NO_2$. ClNO is a known product of the reaction of chloride ion with *sym*-$N_2O_4$ (dimer of $NO_2$)[30] and its release into the atmosphere was suggested from the reaction of moist NaCl with nitrogen dioxide.[31] Early experiments with relatively high levels of $NO_2$ reacting with wet or dry NaCl showed the formation of ClNO.[32] Subsequently it was demonstrated that nitrosyl chloride was produced when even ppm levels of $NO_2$

[a] *Department of Chemistry, University of Illinois at Chicago, Chicago, Illinois 60607, USA. E-mail: audreydh@uic.edu*
[b] *Department of Chemistry, University of California Irvine, Irvine, California 92697, USA*
[c] *Institute of Chemistry and the Fritz Haber Research Center, The Hebrew University, Jerusalem, 91904, Israel*
[d] *Laboratory of Physical Chemistry, FIN-00014 University of Helsinki, Finland*

† Electronic supplementary information (ESI) available: Structures of model compounds; *ab initio* electronic and AIMD structural data for $N_2O_5$, selected water clusters, and $N_2O_5$ adsorbed onto a thin film of water; properties of water slab film model and slab with an $N_2O_5$ adsorbate. See DOI: 10.1039/c5cp02664d

reacted with dry NaCl.[33] Both sets of experiments were characterized by a ClNO yield which plateaued suggesting a surface controlled reaction. Furthermore, more recent studies indicate that ClNO, too, is produced in a water-mediated reaction when $NO_2$ reacts with wet or dry HCl.[19] Unfortunately the detection and quantification methodology does not currently exist to confirm the existence of ClNO in the ambient atmosphere.

Ionic species have been invoked in mechanisms proposed for the hydrolysis of $N_2O_5$ and the hydrolysis of $NO_2$ in the atmosphere. $N_2O_5$ forms an ionic crystal with distinct nitronium and nitrate ions ($NO_2^+$ and $NO_3^-$).[34] The nitronium ion is a well-known electrophile in nitration reactions.[35] In early experiments on the hydrolysis of $N_2O_5$ on $NH_4HSO_4$ aerosol particles[36] it was postulated that the mechanism included the disproportionation of $N_2O_5$ as its second step:

$$N_2O_5(g) \Leftrightarrow N_2O_5(aq)$$

$$N_2O_5(aq) \rightarrow NO_2^+(aq) + NO_3^-(aq)$$

$$NO_2^+(aq) + H_2O(l) \rightarrow H^+(aq) + HNO_3(aq)$$

$$NO_3^-(aq) + H^+(aq) \Leftrightarrow HNO_3(aq)$$

$$HNO_3(aq) \Leftrightarrow HNO_3(g) \quad (1)$$

This mechanism was adapted to the reaction of $N_2O_5$ with NaCl solutions[37] where the $NO_2^+$ ion from $N_2O_5$'s disproportionation reacts directly with chloride to form $ClNO_2$ in an alternate third step to eqn (1). Laboratory experiments on surface adsorbed $N_2O_5$ give a clear spectroscopic signature for the nitronium cation which diminishes upon addition of dry HCl.[19]

Ionic forms may also play a prominent role in the chemistry of $NO_2$. In the gas phase $NO_2$ and its symmetrical dimer, $N_2O_4$, are at equilibrium. $N_2O_4$ has a greater attraction for water than $NO_2$ as indicated by $N_2O_4$'s factor of $\sim$100 larger Henry's Law constant[38–44] and would be expected to more preferentially adsorb onto an aqueous surface. $N_2O_4$ is known to isomerize to an asymmetric isomer $ONONO_2$[45–47] which can form an ionic species with nitrosyl and nitrate ions ($NO^+$ and $NO_3^-$).[48] A new comprehensive mechanism for the hydrolysis of $NO_2$ was proposed,[49] consistent with these facts and a majority of prior experimental data. Among the features of this mechanism are (1) the asymmetric $ONONO_2$ isomer of $N_2O_4$ is the key intermediate, (2) the isomer disproportionates to the reactive nitrosonium nitrate ion pair, $NO^+NO_3^-$, and (3) an aqueous film or surface upon which $ONONO_2$ is adsorbed is required. (Only the mechanistic steps relevant for this current work are noted below.)

$$2NO(g) \Leftrightarrow N_2O_4(g)$$

$$N_2O_4(g) \Leftrightarrow N_2O_4(surf)$$

$$N_2O_4(surf) \Leftrightarrow ONONO_2(surf)$$

$$ONONO_2(surf) \Leftrightarrow NO^+NO_3^-(surf)$$

$$NO^+NO_3^-(surf) + H_2O(surf) \Leftrightarrow HONO(surf) + HNO_3(surf) \quad (2)$$

This mechanism is extended to the atmospheric production of ClNO from the reaction of $NO_2$ with HCl upon replacing water in the last step of eqn (2) with HCl.[19]

Only a limited number of theoretical studies have addressed production of these nitrogen oxychlorides and all the models employed make chemical inferences based upon examining the behavior of $N_2O_5$ or $ONONO_2$ in small water clusters containing, at most, a few water molecules. It is not clear whether such models can properly represent the heterogeneous chemistry of these reactions. Here a more substantive treatment of the aqueous surface is undertaken by direct simulation at the molecular level by *ab initio* molecular dynamics (AIMD) simulations where the electronic degrees of freedom are explicitly treated employing density functional theory (DFT). The simulations follow the course of the reaction when gaseous HCl collides with the surface of a thin film of water upon which one of the target dinitrogen oxides is adsorbed. It examines two steps in the mechanisms – for nitryl chloride:

$$N_2O_5(surf) \Leftrightarrow NO_2^+NO_3^-(surf)$$

$$NO_2^+NO_3^-(surf) + Cl^-(surf) \Leftrightarrow ClNO_2(g) + NO_3^-(surf) \quad (3)$$

and for nitrosyl chloride:

$$ONONO_2(surf) \Leftrightarrow NO^+NO_3^-(surf)$$

$$NO^+NO_3^-(surf) + Cl^-(surf) \Leftrightarrow ClNO(g) + NO_3^-(surf) \quad (4)$$

The obvious parallels in the proposed chemistry leading to $ClNO_2$ and ClNO prompts this current work. A main objective is to elucidate the similarities and differences in the chemistry leading to formation of these $ClNO_x$ compounds and to estimate the efficiency of the reactions. An atomistic simulation of the process is employed to give a more realistic description of the thin water film. This will allow the role of the water surface to be deduced and the mechanism for formation of the particular nitrogen oxychloride to be captured in real time. To address the objectives, the paper is structured as follows. First, relevant electronic structure studies of the $N_2O_5$ and $N_2O_4$ systems are discussed. Then the computational details of this study are given. The main attributes of reaction are shown: broken and formed bonds and redistribution of charge. To give a perspective to the reactions, the structure and dynamics of the dinitrogen oxides on an aqueous surface are examined. Charge separation within the oxide and incipient ion pair formation are addressed throughout. Finally the paper summarizes its major findings in the conclusions.

## Models and methodology

*Ab initio* molecular dynamics is particularly well suited to examine chemical reactions where bonds can form and be broken.[50–56] For AIMD simulations modeling a macroscopic

system, a DFT calculation utilizing the appropriate functional on a slab geometry with periodic boundary conditions is one of few practical options. However, relatively few AIMD studies have been published on the $N_2O_5$ or $N_2O_4$ systems. A majority of the reported simulations utilize a dynamic reaction path (DRP) or another similar approach. AIMD simulations at the MP2/6-311++G(d,p) and MPWB1K/6-311++G(d,p) levels of theory on collision of a protonated water molecule with $N_2O_5$ yielded proton transfer from $H_3O^+$ to $N_2O_5$ followed by prompt dissociation of the protonated dinitrogen oxide intermediate, leaving $HNO_3$, $NO_2^+$, and $H_2O$ with the Mulliken charge of the $NO_2^+(H_2O)$ species being $\sim$0.9 a.u.[57] An MP2/DZV DRP investigation of $ONONO_2$ in clusters of 0–8 $H_2O$ molecules showed a dramatic enhancement in extent of ionization with number of waters in the cluster. Only partial ionization was observed with one or two waters and a substantial amount with eight, where Mulliken charges on the N atoms were +0.74 and $-$0.79 a.u.[58] When examined with a higher level of theory with optimized geometries, an MP2/SOS-RIMP2/aSVP AIMD study with four waters exhibited a maximum charge separation, obtained *via* natural population analysis, between the NO and $NO_3$ moieties of 1.5 a.u. where it was shown that this corresponded to a local minimum, significantly charge separated but not yet with a charge difference of 2 a.u. expected for an ion pair.[59] The same system, examined at the BLYP-D/TZVPP level of theory, displayed a Mulliken charge separation of 0.88 a.u.[60] A dynamic B3LYP/6-31G study based on gradients and Hessians indicated that clusters of symmetric $N_2O_4$ with 0–7 $H_2O$ isomerized to the asymmetric $ONONO_2$ isomer in water assisted as well as non-water assisted pathways and suggested the participation of $NO^+NO_3^-$.[61] Clusters of $ONONO_2$, HCl, and 0–2 waters in DRP MP2/cc-pVDZ simulations yielded a mechanism where hydrogen bonded water forms a proton wire for $H^+$ transfer from HCl to water to the $NO_3$ moiety forming $HNO_3$ and nitrosyl chloride.[19,62] In our previous work the formation of ClNO was observed in AIMD molecular dynamics simulations of $ONONO_2$ adsorbed onto a thin film of water whose surface was struck by gaseous HCl.[63]

Many electronic structure studies have been performed on $N_2O_5$ and $N_2O_4$[64–83] providing information on equilibrium geometries, electronic and thermodynamic parameters, and spectroscopic properties. A summary of relevant DFT and non-DFT equilibrium geometries for $N_2O_5$ can be found in Tables S1 and S2 of the ESI.† The summary data for the asymmetric $N_2O_4$ isomer, *cis*-$ONONO_2$, is available in our prior work.[63] These data indicate that in the gas phase $N_2O_5$ has each of its terminal $NO_2$ groups in a nearly planar $NO_3$ configuration with the bridging oxygen atom where the planes are twisted $\sim$68° with respect to one another (34° torsion angle) and has an N–O–N bridge with somewhat long ($\sim$1.5 Å) N–O bonds. A few studies have addressed the effect of water by examining the dinitrogen oxide in a small water cluster[58,59,61,84–88] or by trying to incorporate the effect of bulk water.[89–91] Some have added HCl to the cluster.[19,62,92] The effect of the size of the water cluster on the geometry of $N_2O_5$ given by these studies relevant to this work is shown in Table S3 of the ESI† with the complimentary data for $N_2O_4$ in our previous study. Fig. S1 (ESI†) gives the structures of $N_2O_5$ and its clusters with 1, 2, and 4 water molecules.

For both dinitrogen oxides the cluster studies show that the size of the water cluster has a large influence on the geometry of the oxide and effects polarization, suggesting an incipient ionization. Nevertheless, as will be demonstrated for the current two systems, the cluster studies are best considered akin to one of many local configurations available to a system immersed in an extended aqueous surface, albeit lacking in the full extent of the ionization capabilities and dispersion provided by the extended surface. As such, they can overestimate the effect of proton transfer processes when a strong acid such as HCl is present in the cluster. This is apparent in the dinitrogen oxide/HCl/water cluster studies reported.[19,62,92] In this case the limited size of the cluster precludes extrapolation of behavior beyond the reduced dimensionality physical model which a cluster represents. Aside from our work on $ONONO_2$, we are unaware of any AIMD study which explicitly incorporates a water surface upon which $NO_{x/y}$ chemistry can evolve. New results on that system will be compared with the $N_2O_5$ reaction to show the similarities and unusual differences in the chemistry which lead to formation of the requisite nitrogen oxychloride.

## Computational details

The AIMD simulations reported here are performed with the CP2K suite of programs (CP2K website: http://www.cp2k.org). The Quickstep module[93] is employed to calculate the electronic structure; it adopts a hybrid basis set of Gaussian and plane waves for *ab initio* Born–Oppenheimer molecular dynamics within the Kohn–Sham framework of density functional theory.[94,95] The Becke–Lee–Yang–Parr DFT functional[96,97] is used incorporating the Grimme dispersion correction,[98,99] BLYP-D3. The Kohn–Sham orbitals are expanded in terms of contracted Gaussian functions with a triple $\zeta$ doubly polarized TZV2P valence basis set. The auxiliary basis set of plane waves is defined by a 280 Ry electron density grid. The interaction between valence electrons and the frozen atomic cores is replaced by norm-conserving Goedecker–Teter–Hutter atomic pseudopotentials optimized for BLYP.[100] Elements of the Kohn–Sham and overlap matrices less than $10^{-12}$ are neglected and convergence of the SCF wavefunction is subject to a criterion of $10^{-6}$ placed upon the electronic gradient. The nuclear equations of motion are integrated using the velocity Verlet algorithm with a 0.5 fs time step.

In the AIMD simulations the thin film of water is modeled by a slab of water constructed from a rectangular box whose dimensions are 13.47 by 15.56 with the *z*-axis varying between 38 and 48 Å. Periodic boundary conditions are employed in *xy* with the free *z* dimension maintained to exceed more than twice the atomic layer. Periodic images are electrostatically decoupled by utilization of the Martyna–Tuckerman Poisson solver.[101] The slab of 72 deuterated water molecules is equilibrated at the desired temperature for at least 40 ps in the canonical ensemble. (All H in the simulations are deuterated to enable a larger timestep and lessen nuclear quantum effects.) Upon equilibration, a geometry optimized molecule of the dinitrogen oxide is placed on top of the slab surface and an

 

additional equilibration of at least 20 ps performed in the *NVT* ensemble. To simulate collision with the slab surface, a geometry optimized HCl molecule is placed in one of three different orientations 4.5–6.5 Å above the slab's Gibbs dividing surface, $z_{GDS}$, and the system subject to a 2 ps *NVT* with the $z$ dimension of HCl constrained at its initial placement above $z_{GDS}$. Finally, collision is initiated by imparting 1, 2, or 4 kT of collision energy at the start of a microcanonical simulation. Many 10–80 ps *NVE* trajectories are collected.

When corrected for dispersion, the generalized gradient approximation functionals used in DFT have been shown to yield a good description of water in a slab geometry as employed in the BLYP-D3/TZV2P description here.[102–104] To assess its performance on the dinitrogen oxides of interest, molecular parameters are obtained for the $N_2O_5$ structures given in Fig. S1 (ESI†) (oxide and selected water clusters) and summarized in Tables S1 and S2 of the ESI.† Complimentary data on $ONONO_2$ is available in our prior work. For both systems the bond lengths/bond angles are generally comparable to those determined from higher levels of theory (distances within 0.02–0.03 Å, angles within 3–4°) with one exception. For $N_2O_5$ the bridge N–O bond (N1–O5 or N2–O5) is 6% longer than the experimental value (1.59 *versus* 1.50) and the N1–O3 bond of *cis*-$ONONO_2$ is 10% higher than the value from a CASSCF(12e/9o)/6-31G(d,p) optimization (1.47 *versus* 1.34 Å).[91] In the latter case this bond is not broken during the reaction so its greater length is expected to have little impact upon ClNO formation.

## Results and discussion

The salient features in the reaction of both dinitrogen oxides with HCl on a thin water slab are exhibited in Fig. 1. First, formation of the new bond and breaking of the old are illustrated. The upper panels follow, in red, the distance between Cl and the oxide N atom that it will eventually react with. Initially chlorine is in gaseous HCl located above the slab surface and finally in the nitrogen oxychloride product given by the horizontal portions of the curves, either $ClNO_2$ or ClNO with average bond lengths near 2 Å. Concurrently, a bridging N–O bond of the oxide is breaking (N2–O5 or N2–O3 in black). In the reactants, the bond is stable; a 1.61 Å bond length in $N_2O_5$ (the turquoise inset in the upper left shows this bond magnified by a factor of 5) or a considerably longer 2.11 Å in *asym*-$N_2O_4$. What appears to be noise in the horizontal portions of all traces is just the response of the bond length to vibrational periods which are on the order of tens of femtoseconds. As the new bond forms, the fragments separate into nitrogen oxychloride and nitrate products. The ensuing N–Cl distance smoothly decreases until the N–Cl bond length of the oxychloride is obtained while the distance between the nitrate oxygen and

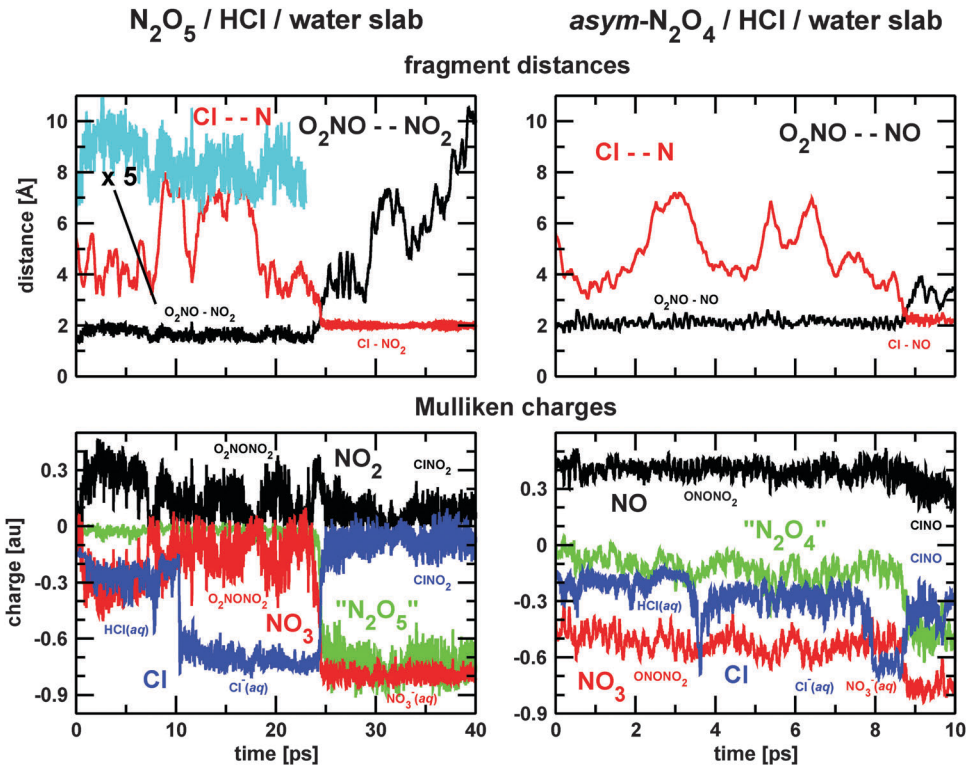


Fig. 1 Time evolution in reactions of $N_2O_5$ and $ONONO_2$ with HCl on the surface of a thin film of water. Top panels: distance between incoming $Cl^-$ ion and N atom being attacked and distance between the nitrogen oxide fragments whose bond is being broken. Turquoise inset in upper left denotes the N–O bond of $N_2O_5$ prior to its reaction magnified by a factor of 5. Bottom panels: Mulliken charges on ions, products, and reactant fragments. Numerical values are given in Table 1. $N_2O_5$ – 52 ps 329 K trajectory with 2 kT of collision energy; $N_2O_4$ – 20 ps 314 K trajectory with 4 kT collision energy.

nitryl or nitrosyl nitrogen smoothly increases, hallmarks of a concerted simultaneous substitution/elimination reaction: $Cl^-$ is coming in to bond with the nitryl or nitrosyl N while the bond lengthens between the nitrogen oxide fragments at the same time until the $NO_3^-$ leaving group is finally expelled. The trajectories give the reaction as occurring at 25 ps on the left and 8.7 ps on the right.

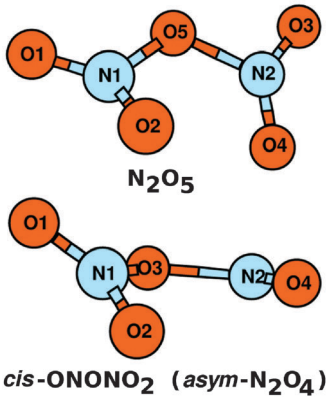


### Charge distribution for reaction

Another quite dramatic means to examine reaction, which can lead to a better mechanistic understanding, is through changes in charge distribution as shown in the lower panels of Fig. 1. Table 1 should be consulted as it gives Mulliken charges found in this study for all ions, reactants, products, and selected fragments in the gas phase, on a water slab, and for the reaction on a water slab. Specific values for partial charges can vary with different theoretical approaches, levels of theory, basis sets employed, and type of population analysis. It is the difference in partial charges which will be most useful in examining the reaction and understanding the electron density distribution which defines sites susceptible to nucleophilic reaction. Starting with Cl (blue trace), it begins covalently bound in gaseous HCl with a partial atomic charge of −0.15 a.u. for both systems examined. Upon striking the aqueous surface, HCl remains molecular, though solvated, and undergoes numerous extremely short lived proton transfer events, the ones at 8 ($N_2O_5$) and 3.8 ps (*asym*-$N_2O_4$) almost successful. Solvent mitigated femtosecond transfer processes reduce the charge to ∼−0.25 a.u. Then at 10 and 8 ps true proton transfer occurs and the charge drops precipitously. As the hydronium ion migrates away *via* proton hopping and the aqueous solvation shell establishes itself, the charge slowly decreases further until solvated $Cl^-$ reaches a charge of −0.72 a.u. for the $N_2O_5$ trajectory. In the particular trajectory on the right, $Cl^-$ reacts with $ONONO_2$ within a picosecond of being liberated. Its solvation shell is neither fully established nor equilibrated, resulting in a somewhat higher $Cl^-$ partial charge. At 25 and 8.7 ps a precipitous increase in Cl charge indicates reaction with the dinitrogen oxide and incorporation into the corresponding nitrogen oxychloride. Clearly, then, it is the chloride ion rather than HCl which is the reactant. Furthermore the acidic proton is not involved in the reaction whatsoever; neither the nitrate nor any other species (save hydronium) is protonated. The proton is independently performing its Grotthuss proton hopping.[105,106]

Table 1 Mulliken partial charges of reactants and products

| Fragment | Gas phase[a] | Water slab[b] | Reaction/slab[c] |
|---|---|---|---|
| $Cl^-$ | | | −0.72 |
| $NO_3^-$ | | | −0.80 |
| HCl: | | | |
| H | 0.15 | | |
| Cl | −0.15 | | −0.26 |
| $ClNO_2$: | | | |
| Cl | −0.08 | | −0.08 |
| $NO_2$ | 0.08 | | 0.06 |
| ClNO: | | | |
| Cl | −0.18 | | −0.27 |
| NO | 0.18 | | 0.26 |
| $N_2O_5$: | | | |
| $N_2O_5$ | 0 | −0.02 | −0.02 |
| $NO_2$ | 0.10 | 0.12 | 0.11 |
| $NO_3$ | −0.10 | −0.14 | −0.13 |
| *cis*-$ONONO_2$: | | | |
| *asym*-$N_2O_4$ | 0 | −0.14 | −0.12 |
| NO | 0.24 | 0.40 | 0.40 |
| $NO_3$ | −0.24 | −0.54 | −0.52 |

[a] Geometry optimized structure (0 K). [b] Dinitrogen oxide adsorbed onto water slab – averaged over 42 ps 278 K, 43 ps 292 K, or 45 ps 322 K trajectories ($N_2O_5$); final 30 ps of a 60 ps 307 K trajectory ($N_2O_4$). [c] From reactions given in Fig. 1.

Fragments of the dinitrogen oxide reactants also exhibit large changes in charge upon reaction. The two $NO_2$ groups of $N_2O_5$ are equivalent and any separation into $NO_2$ and nitrate is arbitrary. Here separation is done by choosing the $NO_2$ moiety that contains the N atom which will eventually form nitryl chloride. Prior to reaction partial charges on the $NO_2$ (in black in lower panel of Fig. 1) and $NO_3$ fragments (in red) exhibit high as well as low frequency components. The high frequency component appears as "noise" in each trace and has a timescale of femtoseconds. The low frequency component gives rise to the picosecond timescale oscillations observed in the $NO_2$ and $NO_3$ partial charges before the reaction at 25 ps. Both components are perfectly correlated with motion in the $O_2NO$–$NO_2$ bond (N2–O5) as comparison of the $NO_2$ charge in the lower left panel with the magnified (×5) bond length in the turquoise inset of the upper left panel demonstrates. The high frequency oscillations are attributable to vibrations of the bonds. The low frequency oscillations, whose numerical values achieve a maximum and minimum of approximately 0.47 and −0.51 a.u., have average magnitudes of only a little in excess of 0.1 a.u., slightly more than the gas phase species as evidenced in Table 1. They will be examined more fully later. As the two terminal $NO_2$ groups are equivalent and the charge is oscillatory prior to reaction, the values reported are obtained by assigning the $NO_2$ and $NO_3$ fragments to each N and then averaging over the first 24 ps of the trajectory. This yields an average charge separation between the fragments of 0.24 a.u. $N_2O_5$ is a neutral molecule and consequently one would expect its fragments to sum to zero. Their sum is given by the green

 

curve in the lower panel, sum of all partial atomic charges of atoms in the original molecule prior to reaction, "$N_2O_5$". What is observed in the horizontal portion of the green curve before the reaction at 25 ps is a small net negative charge, −0.02 a.u., indicating a low level of charge transfer from surrounding waters. This small charge is consistently observed in all trajectories. The reaction is a somewhat rare event, commencing at a point when the charge on the $NO_2$ fragment and the $O_2NO$–$NO_2$ bond length are at maxima and the $NO_3$ fragment charge at a minimum. Upon reaction, while the product $NO_2$ fragment charge (in $ClNO_2$) does not significantly differ from that of the reactant $NO_2$ as shown in black, the $NO_3$ of the nitrate product carries far more electron density than the $NO_3$ fragment of the reactant (red trace). $NO_3^-$ and product fragment charges are taken from averaging the trajectory to 52 ps. Notice that the two ions ($Cl^-$ and $NO_3^-$) do not bear a full a.u. of charge due to charge transfer to surrounding waters. Mulliken charges less than unity have been reported for water clusters and bulk aqueous solutions containing these anions: −0.65 to −0.86 for $Cl^-$ and −0.90 a.u. for $NO_3^-$.[107–109] The −0.72 and −0.80 a.u. found here for these respective ions (see Table 1) are reasonably consistent.

$ONONO_2$ can naturally be considered as bonded NO and nitrate groups. The lower right panel of Fig. 1 shows that there exists a substantial polarization between these fragments whenever $ONONO_2$ is adsorbed onto an aqueous surface. The charge separation of almost 1 a.u. has doubled its gas phase value (see Table 1). The observed 0.92–0.94 a.u. charge separation is in good agreement with a value of 0.88 determined on a cluster of *cis*-$ONONO_2$ with 4 waters.[60] But in contrast to dinitrogen pentoxide, the charge on each fragment is rather constant (except for the vibrational motions) until reaction at 8.7 ps. In addition, their sum given by the green "$N_2O_4$" curve averages to −0.12 a.u.; a nontrivial density of electrons has transferred from surrounding waters. After reaction the NO of ClNO is found to bear somewhat less charge than in the reactant and the nitrate ion a charge comparable to the $NO_3^-$ liberated from $N_2O_5$. The NO, "$N_2O_4$", HCl, and $NO_3$ charge values are obtained from averaging the trajectory to 8 ps and the $NO_3^-$ and product fragment charges from averaging to 20 ps.

### Dinitrogen oxides on thin water films

The atmospheric surfaces upon which the reactions of this study actually take place are undoubtedly not uniform slabs of water, some may involve pools of water or even be thinner than the slabs constructed here.[6] The aim of this work is to create a realistic model for an aqueous surface which has the necessary mobility and is not overstructured exploiting the known good DFT description afforded to water and the liquid/vapor interface by BLYP-D3/TZV2P.[102–104] Fig. S2 in the ESI† gives the density profile and diffusive behavior of the aqueous slab and the slab with the $N_2O_5$ adsorbate. The figure indicates that the slab exhibits the desired mobility and does not suffer from overstructuring. The first peak in the pair correlation function for the water oxygen atoms and the orientation of the water dipoles in the upper and lower slab surfaces both yield normal behavior.

Examination of the dynamical and structural properties of each of the dinitrogen oxides adsorbed alone upon the surface of a slab may clarify the simulated reactions and help elucidate the special role that water assumes. Upper panels of Fig. 2 give the evolution in time of Mulliken charge. Both systems display the same charge magnitudes prior to reaction as given in Fig. 1. In particular, dinitrogen pentoxide exhibits oscillations in fragment charge in the left panel whose 0.11 and −0.13 average values are nearly identical to those of the reacting trajectory as is the sum of −0.02 a.u. for a small level of charge transfer from water. The asymmetric $NO_2$ dimer portrayed on the right shows a constant charge separation between fragments and a level of charge transfer from water similar to the reactive trajectory. Over the course of the last 30 ps of the trajectory the −0.14 a.u. charge transfer from water is observed to be due to the interaction of a nearby water oxygen with the nitrosyl nitrogen. Similar behavior was reported for an MP2/DZV dynamic reaction path study of $ONONO_2$ in a cluster with 8 waters.[58] Numerous studies of $N_2O_5$ given in Table S4 (ESI†) show that an intermolecular interaction of a water oxygen with the nitryl nitrogen of increasingly shorter range ensues as the number of waters in the cluster increases. Table 1 summarizes the Mulliken partial charges for the geometry optimized gas phase species, water slab with adsorbate, and adsorbate on a water slab which is struck by HCl. The two systems studied exhibit significant differences in fragment charge separation on going from the gas phase to the water slab. For *asym*-$N_2O_4$ the approximately 1 a.u. difference for an aqueous surface doubles the gas phase separation value. Yet for $N_2O_5$ the small difference, especially for the reacting trajectory, might be attributable to random noise were it not for the consistency in all trajectories of the −0.02 a.u. water charge transfer. Note that the water slab values for $N_2O_5$ are averaged over three trajectories spanning a 45° temperature range. Obviously average Mulliken fragment charge values show no difference, not even a temperature effect.

While average charge values for $N_2O_5$ are temperature independent there may still be periodicity in its fragment charges. The periodicity of interest is that of the low frequency motion encountered in the fragment charges for $N_2O_5$. The gas phase values of 0.10 and −0.10 a.u. reported in Table 1 are from a geometry optimization at 0 K. *NVE* trajectories of 21 and 22 ps duration of gaseous $N_2O_5$ at 158 and 357 K fail to exhibit any oscillations in fragment charges except for the tens of femtoseconds vibrational motion and yield average charges identical to the 0 K values. As this suggests the importance of the aqueous surface, three well equilibrated *NVE* trajectories were obtained of slabs with an $N_2O_5$ adsorbate over a 45° temperature range. The time evolution of Mulliken fragment charge for these greater than 40 ps *NVE* simulations are portrayed in Fig. S3 of the ESI.† They all show 0.12, −0.14 average fragment partioning and −0.02 a.u. transfer from water, as found in Fig. 1 for the reactive trajectory prior to reaction. There is a slight increase in magnitude of the high frequency oscillations with temperature, as would be expected. Importantly, the figure

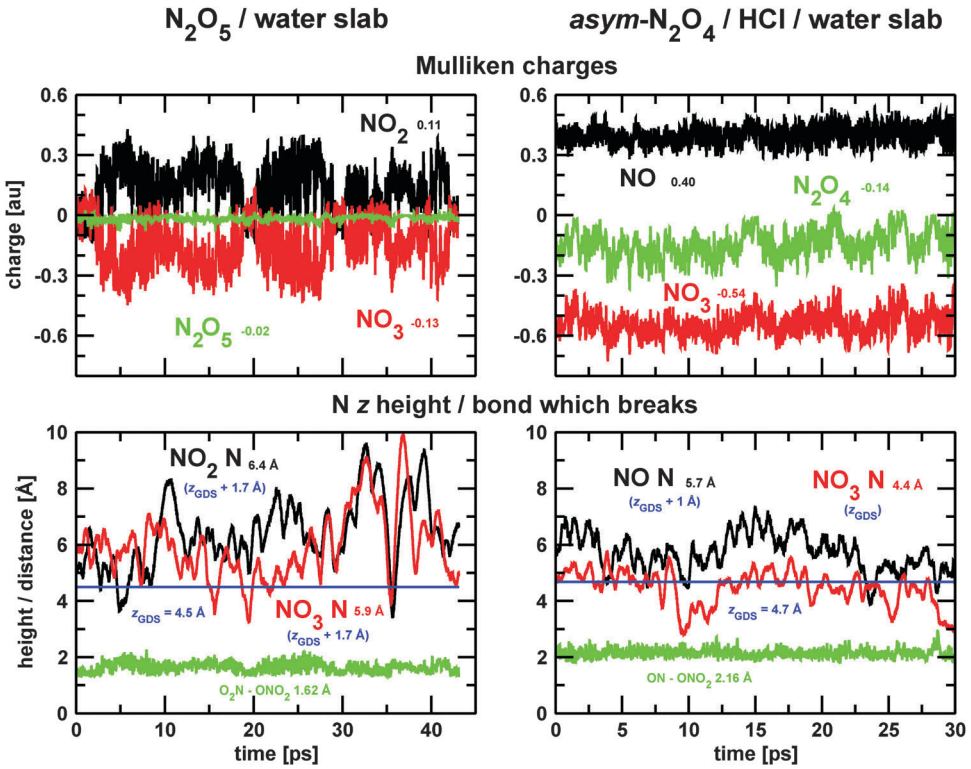


Fig. 2 Time evolution of $N_2O_5$ and $ONONO_2$ adsorbed onto the surface of a thin film of water. Top panels: Evolution of Mulliken charge on nitrogen oxide fragments, green curves on the molecule. Bottom panels: Temporal behavior in *z* height above surface of N atoms in each oxide, included is the fragment bond which will break, green curve. $N_2O_5$ – final 43 ps of a 48 ps 322 K trajectory; $N_2O_4$ – final 30 ps of a 60 ps 307 K trajectory.

exhibits an unambiguous temperature dependence in $NO_2$ and $NO_3$ fragment charges with a frequency which increases with increasing temperature. Furthermore, analysis of the actual values of the fragment charge separation (not the averages) shows that they decrease with increasing temperature (0.68 at 278 and 0.58 a.u. at 322 K). Periods of approximately 45, 16, and 10 ps are observed for the respective 278, 292, and 322 K trajectories. The fact that the period and charge separation increase as the temperature is lowered exhibits the proper limiting physical behavior: at low temperatures $N_2O_5$ is an ionic solid consisting of discrete $NO_2^+$ and $NO_3^-$ ions – two constant fragment charges of unit magnitude and of infinite period. The formation of ionic nitronium nitrate has been characterized in the low temperature $N_2O_5$ deposition onto various salt or metal substrates and even an ATR infrared crystal,[19,110–112] underpinning the importance of a surface to the chemistry of dinitrogen pentoxide.

Significant structural changes accompany adsorption of either of the dinitrogen oxides upon a thin aqueous film as delineated in Table S3 of the ESI.† (Gas phase and slab data for both $N_2O_5$ and *asym*-$N_2O_4$ are presented.) These changes lead to a relaxation of gas phase structure with enhanced fragment charge separation forming a species more amendable to reaction. For dinitrogen pentoxide changes in bond length/angle are correlated with charge separation. In Fig. 1 it was noted that the amplitude of the time dependence in $O_2NO$–$NO_2$ bond length displays a periodic motion exactly parallel to oscillations in $NO_2$ and $NO_3$ fragment charges. As such, equilibrium values reported in Table S3 (ESI†) are averaged over the $NO_2^{\delta+}$ and $NO_3^{\delta-}$ character which each N atom periodically possesses. To capture the reactive state, structural properties of a fragment with its maximum $NO_2^{\delta+}$ character and another with its maximum $NO_3^{\delta-}$ character need to be examined. Table 2 summarizes some major structural changes $N_2O_5$ and *asym*-$N_2O_4$ undergo in passing from the vapor to an aqueous surface. Data for charged fragments derive from analysis of the 278, 292, and 322 K *NVE* trajectories discussed in the previous paragraph. As both dinitrogen oxides form nitrate as a product, bond lengths and angles of the solvated $NO_3^-$ ion given by the BLYP-D3/TZV2P description of this study are used for comparison as a first approximation to assess $NO_3^-$

Table 2 Water-induced structural changes

| Species | Bridge N–O[a] | $NO_2$ N–O[b] | $NO_2$ ∠[b] |
|---|---|---|---|
| $O_2NONO_2$[c] | | | |
| Gas | 1.59 | 1.21 | 134 |
| $NO_2^{\delta+}$ | 1.79 | 1.19 | 139 |
| $NO_3^{\delta-}$ | 1.47 | 1.23 | 130 |
| $ONONO_2$ | | | |
| Gas | 1.74 | 1.23 | 130 |
| Slab | 2.16 | 1.26 | 123 |
| $NO_3^-$(aq) | | 1.28 | 120 |

[a] N2–O5 or N2–O3 in structural figure. [b] Bond length/angle of terminal $NO_2$ group. [c] Rows 2 and 3 are fragment values from a slab.

character of the oxide. In gas phase $N_2O_5$ the $ONO_2$ fragment's terminal $NO_2$ groups have an N–O bond length and angle (1.21 Å, 134°) further removed from the nitrate ion values of 128 Å and 120° than *asym*-$N_2O_4$ (1.23 Å, 130°), suggesting greater changes in geometry are required were an ion pair to form. Upon adsorption onto a slab the equivalence and symmetry of the two $NO_2$ groups is broken by the dynamic asymmetric environment the aqueous surface affords. Though small, the $NO_2^{\delta+}$ fragment has bond lengths which shorten and an angle which increases while the opposite behavior is demonstrated by the $NO_3^{\delta-}$ fragment. The extension and contraction of the bridge N–O bond is significant for both fragments. On the other hand for $ONONO_2$, the $ONO_2$ fragment's $NO_2$ group has an N–O bond and angle which moves to within 0.02 Å and 3° of nitrate's and the bridge N–O bond between fragments considerably lengthens. More modest, though still significant, increases of the bridge bond length have been reported in small cluster studies[58,59,91] and a larger value of 2.23 Å reported for a CASSCF(12e/9o)/6-31G(d,p) quantum mechanical/molecular mechanics (QM/MM) study with QM *asym*-$N_2O_4$ and two $H_2O$ in a box of 279 classical waters.[91] Both oxides exhibit structural changes and charge separation upon a thin aqueous film which promotes reactivity. But *asym*-$N_2O_4$ shows more ion pair character.

In addition to fragment charge periodicity and structural parameters, the bottom panels of Fig. 2 indicate another difference between the $N_2O_5$ and *asym*-$N_2O_4$ systems. The nitryl and nitrate fragments of $N_2O_5$ exhibit large variations in position above the slab surface, averaging more than 1.5 Å above $z_{GDS}$ and, for this 43 ps trajectory, have the same average height. (Given the large amplitude motion a trajectory including many more periods is required to obtain a converged value for the $z$ free dimension.) The consistency in height of the N atoms is maintained as temperature is varied as Fig. S3 of the ESI† demonstrates. The only effects observed with increasing temperature are an expansion of the slab causing an increase in $z_{GDS}$ and more pronounced motion of the fragments resulting in higher average positions above the interface. No meaningful difference in height of the N atoms of the $NO_2$ or $NO_3$ fragments is found indicative of the long time equivalence of the two nitryl groups. In *asym*-$N_2O_4$ the $ONONO_2$ nitrate N is basically at the liquid/vapor interface and the nitrosyl N, on average, an angstrom above. Consequently, the nitrate fragment's oxygens are well positioned in the interface to enable efficient hydrogen bonding from adjacent water molecules. This fosters stabilization of the nitrate fragment when the nitrosyl nitrogen reacts with $Cl^-$. Mulliken charges on the nitrate O atoms of gaseous $ONONO_2$ all differ with a maximum difference of 0.1 a.u. On the slab they basically all bear the same charge (average of −0.38) with a maximum difference of less than 0.04 a.u. The O atoms of the solvated $NO_3^-$ ion average 0.45 a.u. On an aqueous surface *asym*-$N_2O_4$ exhibits significant ion pair character.

A final comment on ion pair formation. Trajactories greater than 20 ps in length of *cis*-$ONONO_2$ on a water slab exhibit isomerization to the *trans* isomer. On several occasions the bond between NO and $NO_3$ fragments breaks, the NO group migrates to another $NO_3$ oxygen, and a new bridge N–O bond forms. Never does the separation between the N atoms have a significant extension beyond 3 ± 0.1 Å (maximum fluctuation of 3.5; minimum of 2.7 Å during *cis* → *trans*, migration periods) nor is a water molecule seen to intercede between fragments. As the migrating group is actually $NO^+$, this behavior indicates at least transitory existence of an ion pair. An electronic structure study of several $NO_2$ dimers carried out with high level *ab initio* methods indicated that density functional theory employing the B3LYP functional erroneously gives a stable $NO_3^-$ and $NO^+$ ionic pair intermediate during *cis*/*trans* isomerization of *cis*-$ONONO_2$.[83] Consequently, the dynamics of $ONONO_2$ on the slab were closely examined and reveal two distinct sets of behavior. (1) Isomerization is characterized by a transition-like state with an N1O3N2O4 dihedral angle of 72° [69°] and distances of the nitrosyl N to the two nearest $NO_3$ O atoms of 1.96 [1.78] and 2.70 [2.58] Å. (2) Migration initiates from the *trans* isomer and exhibits a transition-like state with an N1O3(O1)N2O4 dihedral angle of 113° [113°] and equal distances of 2.19 [2.00] Å for the nitrosyl N and the two nearest O atoms of the $NO_3$ fragment. Considering that the nitrate fragment participates in hydrogen bonding to adjacent waters and the nitrosyl N interacts with O atoms of nearby water molecules, these transition-like states compare favorably with the high level electronic structure study whose values are given in brackets.[83] For the $N_2O_5$ system only a single case of $NO_2^+$ migration is observed.

## Conclusions

*Ab initio* molecular dynamics simulations are employed to follow the course of two important atmospheric reactions enabling elucidation of their mechanisms within BLYP-D/TZV2P density functional theory. Both of these heterogeneous reactions involve adsorption of a dinitrogen oxide upon a thin film of water which gaseous HCl impinges. The reaction of $N_2O_5$ produces $ClNO_2$ (nitryl chloride) and nitrate ion while *cis*-$ONONO_2$ forms ClNO (nitrosyl chloride) and nitrate. Both nitrogen oxychlorides result from a three-step $S_N2$ mechanism where water assumes a preeminent role. (1) An aqueous surface activates the adsorbed dinitrogen oxide for reaction. (2) Water ionizes the impinging gaseous HCl to produce the $Cl^-$ nucleophile. (3) In a concerted water-mitigated reaction $Cl^-$ attacks the electrophilic oxide N atom while nitrate is eliminated. Water is involved in every aspect of the reaction – from tethering the adsorbed oxide so that it is physically accessible for reaction to providing a polar reservoir for transfer of electron density to, from, as well as within the oxide, facilitating charge transfer between fragments to the point of ion pair formation, enhancing the electrophilicity of the N atom to be attacked. The simulations exhibit a difference in the manner in which the $S_N2$ mechanism is initiated for $N_2O_5$ and *asym*-$N_2O_4$. $ONONO_2$ undergoes a straightforward, classic $S_N2$ process where mere adsorption onto an aqueous surface is sufficient

to induce the large separation of charge between $NO^{\delta+}$ and $NO_3{}^{\delta-}$ fragments forming the electrophilic N to be attacked. On the other hand, $N_2O_5$ has two nitryl groups, $O_2N–O–NO_2$, whose equivalence precludes formation of a permanent reactive electrophilic N under the conditions of the simulations. Instead, charge separation oscillates in time between the two nitrogen containing fragments ($NO_2{}^{\delta+}$, $NO_3{}^{\delta-}$ and $NO_3{}^{\delta-}$, $NO_2{}^{\delta+}$). The reaction is not as facile as for the *cis* isomer requiring that one of the nitryl groups has its maximum $\delta^+$ character while the $Cl^-$ anion is in position to attack.

The mechanisms revealed by this study are unobtainable from small cluster models and may serve as an example of when results from small water clusters do not necessarily extrapolate to the extended aqueous system or surface. In the extended model for an aqueous surface HCl readily ionizes, efficient proton tranfer amongst water molecules exists, and water stabilizes polar and charged species. Incorporation of HCl into an aqueous cluster containing either one of the dinitrogen oxides is dominated by proton transfer to the oxide as the necessary number of waters to foster HCl ionization is absent. Furthermore, the reactivity of the oxide with water in a small cluster may appear enhanced without the stabilization afforded by the dispersion of the larger system.

Species containing reactive halogens, such as nitryl and nitrosyl chloride, are important in the chemistry of the stratosphere and troposphere due to liberation of very reactive halogen free radicals upon photolysis. The heterogeneous reactions leading to their formation need to be defined and verified in order to better understand and assess the regional and global impacts of this chemistry. Laboratory studies demonstrate that $ClNO_2$ is produced by the reaction examined here, nitryl chloride is produced from the reaction of dinitrogen pentoxide with chloride ions in air, and large-scale atmospheric models indicate that $ClNO_2$ is a significant source of Cl radicals. This study predicts the formation of ClNO in a reaction analogous to that of nitryl chloride. Unfortunately a specific and sufficiently sensitive analytical technique for its detection and quantification in the atmosphere is lacking. Hopefully the laboratory and theoretical demonstrations of nitrosyl chloride production may serve as an impetus to develop the requisite analytical methodology.

## Acknowledgements

Discussions with Doug Tobias are very gratefully acknowledged. This work was performed under N.S.F. Grant 0909227 with computational facilities made possible by N.S.F. Grant CHE-0840513. A.D.H. and R.B.G. acknowledge partial support by the Israel Science Foundation Grant No. 114/08.

## References

1 B. J. Finlayson-Pitts, *Res. Chem. Intermed.*, 1993, **19**, 235.
2 B. J. Finlayson-Pitts and J. C. Hemminger, *J. Phys. Chem. A*, 2000, **104**, 11463.
3 B. J. Finlayson-Pitts and J. N. Pitts, *Chemistry of the Upper and Lower Atmosphere - Theory, Experiments, and Applications*, Academic Press, San Diego, 2000.
4 B. J. Finlayson-Pitts, *Chem. Rev.*, 2003, **103**, 4801.
5 A. R. Ravishankara, *Proc. Natl. Acad. Sci. U. S. A.*, 2009, **106**, 13639.
6 B. J. Finlayson-Pitts, *Phys. Chem. Chem. Phys.*, 2009, **11**, 7760.
7 A. Saiz-Lopez and R. von Glasow, *Chem. Soc. Rev.*, 2012, **41**, 6448.
8 C. A. Cantrell, J. A. Davidson, R. E. Shetter, B. A. Anderson and J. G. Calvert, *J. Phys. Chem.*, 1987, **91**, 6017.
9 M. A. Tolbert, M. J. Rossi and D. M. Golden, *Science*, 1988, **240**, 1018.
10 B. J. Finlayson-Pitts, M. J. Ezell and J. N. Pitts, *Nature*, 1989, **337**, 241.
11 F. E. Livingston and B. J. Finlayson-Pitts, *Geophys. Res. Lett.*, 1991, **18**, 17.
12 F. F. Fenter, F. Caloz and M. J. Rossi, *J. Phys. Chem.*, 1996, **100**, 1008.
13 R. C. Hoffman, M. E. Gebel, B. S. Fox and B. J. Finlayson-Pitts, *Phys. Chem. Chem. Phys.*, 2003, **5**, 1780.
14 W. Behnke and C. Zetzsch, *J. Aerosol Sci.*, 1990, **21**, S229.
15 W. Behnke, C. George, V. Scheer and C. Zetzsch, *J. Geophys. Res.*, 1997, **102**, 3795.
16 F. Schweitzer, P. Mirabel and C. George, *J. Phys. Chem. A*, 1998, **102**, 3942.
17 J. A. Thornton, C. F. Braban and J. P. D. Abbatt, *Phys. Chem. Chem. Phys.*, 2003, **5**, 4593.
18 H. D. Osthoff, J. M. Roberts, A. R. Ravishankara, E. J. Williams, B. M. Lerner, R. Sommariva, T. S. Bates, D. Coffman, P. K. Quinn, J. E. Dibb, H. Stark, J. B. Burkholder, R. K. Talukdar, J. Meagher, F. C. Fehsenfeld and S. S. Brown, *Nat. Geosci.*, 2008, **1**, 324.
19 J. D. Raff, B. Njegic, W. L. Chang, M. S. Gordon, D. Dabdub, R. B. Gerber and B. J. Finlayson-Pitts, *Proc. Natl. Acad. Sci. U. S. A.*, 2009, **106**, 13647.
20 J. P. Kercher, T. P. Riedel and J. A. Thornton, *Atmos. Meas. Tech.*, 2009, **2**, 193.
21 A. Thornton, J. P. Kercher, T. P. Riedel, N. L. Wagner, J. Cozic, J. S. Holloway, W. P. Dube, G. M. Wolfe, P. K. Quinn, A. M. Middlebrook, B. Alexander and S. S. Brown, *Nature*, 2010, **464**, 271.
22 L. H. Mielke, A. Furgeson and H. D. Osthoff, *Environ. Sci. Technol.*, 2011, **45**, 8889.
23 T. P. Riedel, T. H. Bertram, T. A. Crisp, E. J. Williams, B. M. Lerner, A. Vlasenko, S.-M. Li, J. Gilman, J. de Gouw, D. M. Bon, N. L. Wagner, S. S. Brown and J. A. Thornton, *Environ. Sci. Technol.*, 2012, **46**, 10463.
24 G. J. Phillips, M. J. Tang, J. Thieser, B. Brickwedde, G. Schuster, B. Bohn, J. Lelieveld and J. N. Crowley, *Geophys. Res. Lett.*, 2012, **39**, L10811.
25 C. J. Young, R. A. Washenfelder, J. M. Roberts, L. H. Mielke, H. D. Osthoff, C. Tsai, O. Pikelnaya, J. Stutz, P. R. Veres, A. K. Cochran, T. C. VandenBoer, J. Flynn, N. Grossberg, C. L. Haman, B. Lefer, H. Stark,

M. Graus, J. de Gouw, J. B. Gilman, W. C. Kuster and S. S. Brown, *Environ. Sci. Technol.*, 2012, **46**, 10965.
26 L. H. Mielke, J. Stutz, C. Tsai, S. C. Hurlock, J. M. Roberts, P. R. Veres, K. D. Froyd, P. L. Hayes, M. J. Cubison, J. L. Jimenez, R. A. Washenfelder, C. J. Young, J. B. Gilman, J. A. de Gouw, J. H. Flynn, N. Grossberg, B. L. Lefer, J. Liu, R. J. Weber and H. D. Osthoff, *J. Geophys. Res.: Atmos.*, 2013, **118**, 10638.
27 Y. J. Tham, C. Yan, L. Xue, Q. Zha, X. Wang and T. Wang, *Chin. Sci. Bull.*, 2014, **59**, 356.
28 T. P. Riedel, G. M. Wolfe, K. T. Danas, J. B. Gilman, W. C. Kuster, D. M. Bon, A. Vlasenko, S.-M. Li, E. J. Williams, B. M. Lerner, P. R. Veres, J. M. Roberts, J. S. Holloway, B. Lefer, S. S. Brown and J. A. Thornton, *Atmos. Chem. Phys.*, 2014, **14**, 3789.
29 G. Sarwar, H. Simon, J. Xing and R. Mathur, *Geophys. Res. Lett.*, 2014, **41**, 4050.
30 P. Gray and A. D. Yoffe, *Chem. Rev.*, 1955, **55**, 1069.
31 A. P. Altshuller and R. A. Taft, *Tellus*, 1958, **10**, 479.
32 W. H. Schroeder and P. Urone, *Environ. Sci. Technol.*, 1974, **8**, 756.
33 B. J. Finlayson-Pitts, *Nature*, 1983, **306**, 676.
34 E. Grison, K. Eriks and J. L. de Vries, *Acta Crystallogr.*, 1950, **3**, 290.
35 G. Oláh, S. Kuhn and A. Mlinkó, *J. Chem. Soc.*, 1956, 4257.
36 M. Mozurkewich and J. G. Calvert, *J. Geophys. Res.*, 1988, **93**, 15889.
37 W. Behnke, C. George, V. Scheer and C. Zetzsch, *J. Geophys. Res.*, 1997, **102**, 3795.
38 J. L. Durham, J. H. Overton and V. P. Aneja, *Atmos. Environ.*, 1981, **15**, 1059.
39 S. E. Schwartz and W. H. White, Solubility equilibria of the nitrogen oxides and oxyacids in dilute aqueous solution, in *Advances in Environmental Science and Engineering*, ed. J. R. Pfafflin and E. N. Ziegler, Gordon and Breach Science Publishers, New York, 1981, p. 1.
40 W. L. Chameides, *J. Geophys. Res.*, 1984, **89**, 4739.
41 L. R. Martin, Kinetic studies of sulfite oxidation in aqueous solution, in *$SO_2$, NO and $NO_2$ Oxidation Mechanisms: Atmospheric Considerations, ed. J. G. Calvert,* Butterworth Publishers, Boston, 1984, p. 63.
42 Y.-N. Lee and S. E. Schwartz, *J. Phys. Chem.*, 1981, **85**, 840.
43 V. M. Berdnikov and N. M. Bazhin, *Russ. J. Phys. Chem.*, 1970, **44**, 395.
44 J. L. Cheung, Y. Q. Li, J. Boniface, Q. Shi, P. Davidovits, D. R. Worsnop, J. T. Jayne and C. E. Kolb, *J. Phys. Chem. A*, 2000, **104**, 2655.
45 W. G. Fateley, H. A. Bent and B. Crawford, *J. Chem. Phys.*, 1959, **31**, 204.
46 I. C. Hisatsune, J. P. Devlin and J. Wada, *J. Chem. Phys.*, 1960, **33**, 714.
47 R. V. St. Louis and B. Crawford, *J. Chem. Phys.*, 1965, **4**, 857.
48 F. Bolduan and H. J. Jodi, *Chem. Phys. Lett.*, 1982, **85**, 283.
49 B. J. Finlayson-Pitts, L. M. Wingen, A. L. Sumner, D. Syomin and K. A. Ramazan, *Phys. Chem. Chem. Phys.*, 2003, **5**, 223.
50 M. E. Tuckerman, K. Laasonen, M. Sprik and M. Parrinello, *J. Phys.: Condens. Matter*, 1994, **6**, A93.
51 D. Marx and J. Hutter, Ab initio molecular dynamics: theory and implementation, in *Modern methods and algorithms of quantum chemistry, Proceedings NIC Series*, ed. J. Grotendorst, John von Neumann Institute for Computing, Julich, Germany, 2000, vol. 3, p. 339.
52 M. E. Tuckerman, *J. Phys.: Condens. Matter*, 2002, **14**, R1297.
53 C. J. Mundy and I.-F. Kuo, *Chem. Rev.*, 2006, **106**, 1282.
54 R. B. Gerber and J. Sebek, *Int. Rev. Phys. Chem.*, 2009, **28**, 207.
55 B. Kirchner, P. J. di Dio and J. Hutter, Real-world predictions from *ab initio* molecular dynamics simulations, in *Multiscale Molecular Methods in Applied Chemistry*, ed. B. Kirchner and J. Vrabec, Top. Curr. Chem., 2012, vol. 307, p. 109.
56 A. A. Hassanali, J. Cuny, V. Verdolino and M. Parrinello, *Philos. Trans. R. Soc., A*, 2014, **372**, 1.
57 S. T. Ishikawa and T. Nakajima, *Int. J. Quantum Chem.*, 2009, **109**, 2143.
58 Y. Miller, B. J. Finlayson-Pitts and R. B. Gerber, *J. Am. Chem. Soc.*, 2009, **131**, 12180.
59 M. E. Varner, B. J. Finlayson-Pitts and R. B. Gerber, *Phys. Chem. Chem. Phys.*, 2014, **16**, 4483.
60 R. B. Gerber, M. E. Varner, A. D. Hammerich, S. Riikonen, G. Murdachaew, D. Shemesh and B. J. Finlayson-Pitts, *Acc. Chem. Res.*, 2015, **48**, 399.
61 D. de Jesus Medeiros and A. S. Pimentel, *J. Phys. Chem. A*, 2011, **115**, 6357.
62 B. Njegic, J. D. Raff, B. J. Finlayson-Pitts, M. S. Gordon and R. B. Gerber, *J. Phys. Chem. A*, 2010, **114**, 4609.
63 A. D. Hammerich, B. J. Finlayson-Pitts and R. B. Gerber, *J. Phys. Chem. Lett.*, 2012, **3**, 3405.
64 A. Stirling, I. Pàpai and J. Mink, *J. Chem. Phys.*, 1993, **100**, 2910.
65 L. Bencivenni, N. Sanna, L. Schriver-Mazzuoli and A. Schriver, *J. Chem. Phys.*, 1996, **104**, 7836.
66 S. Parthiban, B. N. Raghunandan and R. Sumathi, *J. Mol. Struct.*, 1996, **367**, 111.
67 J.-U. Grabow, A. M. Andrews, G. T. Fraser, K. K. Irikura, R. D. Suenram, F. J. Lovas and W. J. Lafferty, *J. Chem. Phys.*, 1996, **105**, 7249.
68 I. Zhun, X. Zhou and R. Liu, *J. Chem. Phys.*, 1996, **105**, 11366.
69 H. Munakata, T. Kakumoto and J. Baker, *J. Mol. Struct.*, 1997, **391**, 231.
70 E. D. Glendening and A. M. Halpern, *J. Chem. Phys.*, 2007, **127**, 164307.
71 F. Bernardi, F. Cacace, G. de Petris, F. Pepi and I. Rossi, *J. Phys. Chem. A*, 1998, **102**, 1987.
72 I. I. Zakharov, A. I. Kolbasin, O. I. Zakharova, I. V. Kravchenko and V. I. Dyshlovoi, *Theor. Exp. Chem.*, 2007, **43**, 66.
73 J. Jaroszyńska-Wolińska, *J. Mol. Struct.*, 2010, **952**, 74.
74 M. L. McKee, *J. Am. Chem. Soc.*, 1995, **117**, 1629.

75 S. S. Wesolowski, J. T. Fermann, T. D. Crawford and H. F. Schaefer, *J. Chem. Phys.*, 1997, **106**, 7178.
76 X. Wang, Q.-Z. Qin and K. Fan, *J. Mol. Struct.*, 1998, **432**, 55.
77 L. P. Olson, K. T. Kuwata, M. D. Bartberger and K. N. Houk, *J. Am. Chem. Soc.*, 2002, **124**, 9469.
78 F. R. Ornellas, S. M. Resende, F. Machado and B. C. O. Roberto-Neto, *J. Chem. Phys.*, 2003, **118**, 4060.
79 Y. Li, *J. Chem. Phys.*, 2007, **127**, 204502.
80 I. I. Zakharov, A. I. Kolbasin, O. I. Zakharova, I. V. Kravchenko and V. I. Dyshlovoi, *Theor. Exp. Chem.*, 2008, **44**, 26.
81 O. B. Gadzhiev, S. K. Ignatov, A. G. Razuvaev and A. E. Masunov, *J. Phys. Chem. A*, 2009, **113**, 9092.
82 H. Beckers, X. Zeng and H. Willner, *Chem. – Eur. J.*, 2010, **16**, 1506.
83 W.-G. Liu and W. A. Goddard, *J. Am. Chem. Soc.*, 2012, **134**, 12970.
84 I. I. Zakharov, *Theor. Exp. Chem.*, 2012, **48**, 233.
85 R. Bianco and J. T. Hynes, *Int. J. Quantum Chem.*, 1999, **75**, 683.
86 J. A. Snyder, D. Hanway, J. Mendez, A. J. Jamka and F.-M. Tao, *J. Phys. Chem. A*, 1999, **103**, 9355.
87 J. P. McNamara and I. H. Hillier, *J. Phys. Chem. A*, 2000, **104**, 5307.
88 A. F. Voegele, C. S. Tautermann, T. Loertingy and K. R. Liedl, *Phys. Chem. Chem. Phys.*, 2003, **5**, 487.
89 A. S. Pimentel, F. C. A. Lima and A. B. F. da Silva, *Chem. Phys. Lett.*, 2007, **436**, 47.
90 A. S. Pimentel, F. C. A. Lima and A. B. F. da Silva, *J. Phys. Chem. A*, 2007, **111**, 2913.
91 G. Luo and X. Chen, *J. Phys. Chem. Lett.*, 2012, **3**, 1147.
92 J. P. McNamara and I. H. Hillier, *Phys. Chem. Chem. Phys.*, 2000, **2**, 2503.
93 J. VandeVondele, M. Krack, F. Mohammed, M. Parrinello, T. Chassaing and J. Hutter, *Comput. Phys. Commun.*, 2005, **167**, 103.
94 P. Hohenberg and W. Kohn, *Phys. Rev.*, 1964, **136**, B864.
95 W. Kohn and L. J. Sham, *Phys. Rev.*, 1965, **140**, A1133.
96 A. D. Becke, *Phys. Rev. A: At., Mol., Opt. Phys.*, 1988, **38**, 3098.
97 C. T. Lee, W. T. Yang and R. G. Parr, *Phys. Rev. B: Condens. Matter Mater. Phys.*, 1988, **37**, 785.
98 S. Grimme, *J. Comput. Chem.*, 2006, **27**, 1787.
99 S. Grimme, *J. Chem. Phys.*, 2010, **132**, 154104.
100 S. Goedecker, M. Teter and J. Hutter, *Phys. Rev. B: Condens. Matter Mater. Phys.*, 1996, **54**, 1703.
101 G. J. Martyna and M. E. Tuckerman, *J. Chem. Phys.*, 1999, **110**, 2810.
102 T. D. Kühne, T. A. Pascal, E. Kaxiras and Y. Jung, *J. Phys. Chem. Lett.*, 2011, **2**, 105.
103 M. D. Baer, C. J. Mundy, M. J. McGrath, I.-F. W. Kuo, J. I. Siepmann and D. J. Tobias, *J. Chem. Phys.*, 2011, **135**, 124712.
104 R. Jonchiere, A. P. Seitsonen, G. Ferlat, M. Saittal and R. Vuilleumier, *J. Chem. Phys.*, 2011, **135**, 154503.
105 N. Agmon, *Chem. Phys. Lett.*, 1995, **244**, 456.
106 A. Hassanali, F. Giberti, J. Cuny, T. D. Kühne and M. Parrinello, *Proc. Natl. Acad. Sci. U. S. A.*, 2013, **110**, 13723.
107 M. Dal Peraro, S. Raugei, P. Carloni and M. L. Klein, *ChemPhysChem*, 2005, **6**, 1715.
108 H. Mishra, S. Enami, R. J. Nielsen, M. R. Hoffmann, W. A. Goddard and A. J. Colussi, *Proc. Natl. Acad. Sci. U. S. A.*, 2012, **109**, 10228.
109 S. G. Ramesh, S. Re and J. T. Hynes, *J. Phys. Chem. A*, 2008, **112**, 3391.
110 I. C. Hisatsune, J. P. Devlin and J. Wada, *Spectrochim. Acta*, 1962, **18**, 1641.
111 T. G. Koch, A. B. Horn, M. A. Chesters, M. R. S. McCoustra and J. R. Sodeau, *J. Phys. Chem.*, 1995, **99**, 8362.
112 J. Agreiter, M. Frankowski and V. E. Bondybey, *Low Temp. Phys.*, 2001, **27**, 890.

 